ADVANCED MATERIALS TECHNOLOGIES
www.advmattechnol.de

Effect of Filler Aspect Ratio on Stiffness and Conductivity in Phase-Changing Particulate Composites

*Amir Mohammadi Nasab, Trevor L. Buckner, Bilige Yang, and Rebecca Kramer-Bottiglio**

Variable stiffness in elastomers can be achieved through the introduction of low melting point alloy particles, such as Field's metal (FM), enabling on-demand switchable elasticity and anisotropy in response to thermal stimulus. Because the FM particles are thermally transitioned between solid and liquid phases, it is beneficial for the composite to be electrically conductive so the stiffness may be controlled via direct Joule heating. While FM is highly conductive, spherical particles contribute to a high percolation threshold. In this paper, it is shown that the percolation threshold of FM particulate composites can be reduced with increasing particles aspect ratio. Increasing the aspect ratio of phase-changing fillers also increases the rigid-to-soft modulus ratio of the composite by raising the elastic modulus in the rigid state while preserving the low modulus in the soft state. The results indicate that lower quantities of high aspect ratio FM particles can be used to achieve both electrical conductivity and stiffness-switching via a single solution and without introducing additional conductive fillers. This technique is applied to enable a highly stretchable, variable stiffness, and electrically conductive composite, which, when patterned around an inflatable actuator, allows for adaptable trajectories via selective softening of the surface materials.

1. Introduction

Materials and structures that can reversibly switch their stiffness between "rigid" and "soft" in response to external stimuli are required in many emerging applications in soft robotics,[1–4] medical devices,[5] the automotive industry,[6,7] and wearable electronics.[8] Specifically in soft robotics, these materials can be used as artificial muscles or stiffness-tunable tendons and ligaments.[9,10] Variable stiffness materials are load-bearing in one or several directions in their rigid state, but when transitioned to their soft and often stretchable state, let their hosting structures undergo shape change. By using variable stiffness materials, complex configurations and motion trajectories can be achieved with a reduced number of actuators in robotic shape-morphing structures.[11,12]

Variable stiffness can be achieved through different methods[1] using granular materials,[13] fluid-polymer composites,[11,14] magnetorheological fluids[6,7] and elastomers,[15] electrorheological fluids,[16] and elastomers,[17] shape memory polymers,[18] shape memory alloys,[12,19,20] thermoplastics,[21] liquid crystal elastomers,[22–24] and phase-changing filler-composites.[3,9,25,26] Among these approaches to achieve variable stiffness, electrically responsive methods, in particular, are advantageous for electromechanical and untethered robotic systems.[27] Exploring electrically actuated methods, magnetorheological and electrorheological systems often require the support of bulky external hardware such as electromagnets and high-voltage power supplies. However, thermally responsive systems, such as phase-changing filler composites empowered with direct Joule-heating (resistive-heating), may enable more compact robotic systems.

Phase-changing filler composites achieve variable stiffness through solid-liquid phase transition of their inclusions, and their variable stiffness property can be tuned based on the choice and volume fraction of the inclusions and the matrix. The incorporation of fillers also enhances mechanical strength, elastic modulus, or thermal conductivity of the composites in most cases. However, achieving electrical conductivity in phase-changing filler composites for direct Joule-heating is a challenge. Recently, several groups have utilized external heaters, such as helical conductive wires and serpentine channels of liquid metal, along with thermally responsive materials, to decrease the stiffness of a structure by increasing the temperatures past the melting point or glass transition temperature of the variable stiffness material.[28,29] As another approach, conductive fillers such as carbon black[30] and graphite[31] have been incorporated into phase-changing or thermoset polymer matrices to impart electrical conductivity, usually resulting in materials with high electrical resistivity but no elastic response.

In a recent work, a three-component particle–fiber–elastomer composite was fabricated with high stiffness tunability and electrical conductivity.[32] Conductive nickel-coated carbon fibers bridge between the spherical particles of a low melting point alloy in the elastomer matrix and create conductive pathways in the material. Although the stiffness tunability range in this work is as high as ≈30×, the presence of rigid nickel-coated carbon fibers limits the material's stretchability to ≈20% in its soft state.

A. Mohammadi Nasab, T. L. Buckner, B. Yang, R. Kramer-Bottiglio
School of Engineering & Applied Science
Yale University
9 Hillhouse Ave., New Haven, CT 06511, USA
E-mail: rebecca.kramer@yale.edu

The ORCID identification number(s) for the author(s) of this article can be found under https://doi.org/10.1002/admt.202100920.

DOI: 10.1002/admt.202100920

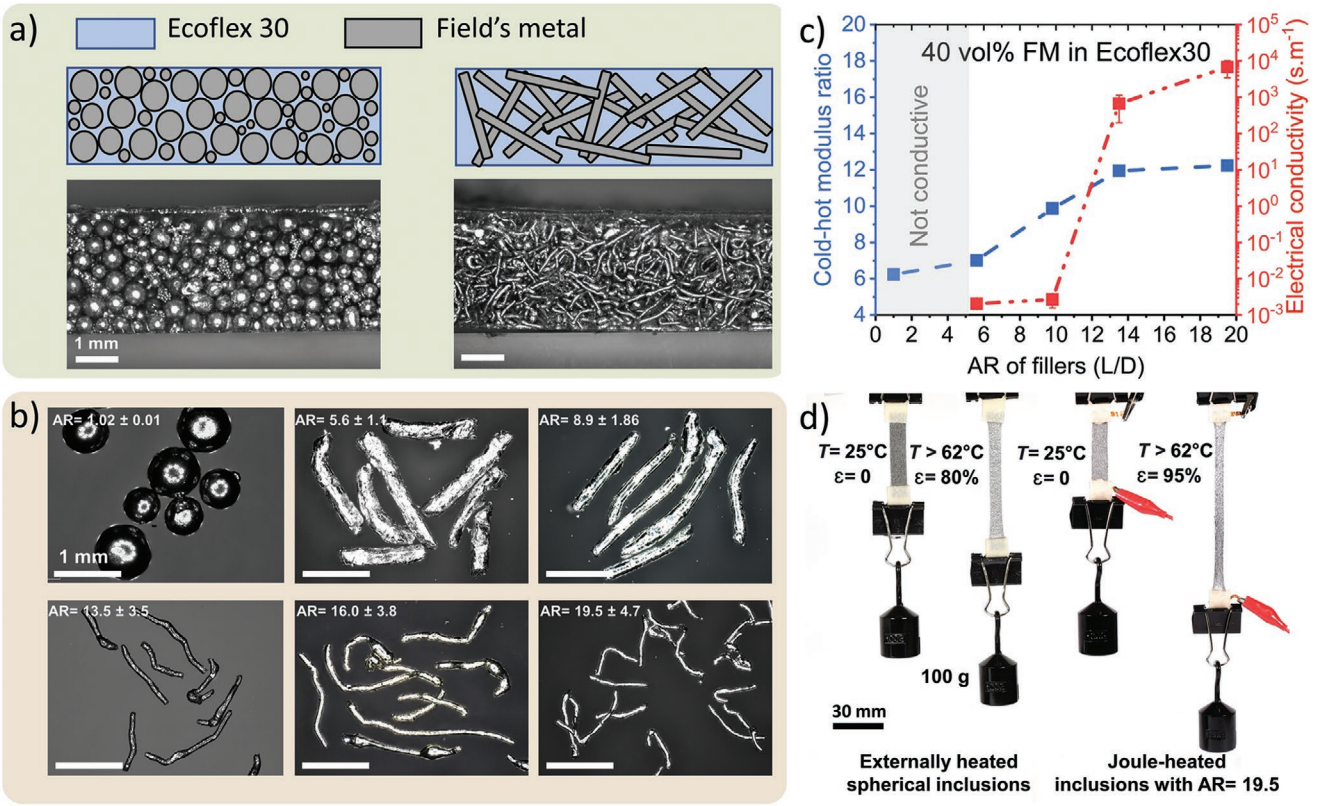

Figure 1. Variable stiffness silicone composite with enhanced electrical and mechanical properties. a) Schematics and microscopic images of silicone composites containing spherical and HAR FM particles. b) Microscopic images of the FM particles with ARs ranging from 1 to 19.5. c) Cold–hot modulus ratio and electrical conductivity of the composites containing Ecoflex 30 and FM particles versus ARs of inclusions at 40 vol% of inclusions. Each data point is acquired based on testing five samples and error bars represent ±1 standard deviation. d) Two specimens of the variable stiffness composites containing spherical (left) and HAR (right) inclusions are shown in the stiff (cold) state, bearing load, and in the soft (hot) state, being stretched. The composites are rigid at room temperature (25 °C) and soft when $T > 62$ °C. An external heat source (heat gun) is needed to soften the composite containing spherical particles, however the composite containing the HAR particles is heated via electrical current applied to both ends of the specimen. Video S1 (Supporting Information) shows the temperature distribution in the sample with HAR particles while being Joule-heated, captured with an IR camera. Both composites here contain 55 vol% FM in Ecoflex 30.

Here, we study filler aspect ratio (AR) as a way to impart electrical conductivity and stiffness-switching via a single solution without introducing additional conductive fillers in phase-changing filler composites. For this study, we adapted our previous variable stiffness material[25] composed of a silicone matrix (Ecoflex 30) and Field's metal (FM; eutectic alloy of bismuth, indium, and tin with a low melting point at T_m = 62 °C) particles. The elastic modulus of FM drastically and rapidly drops from 9.25 GPa[33] when heated above its melting temperature via solid–liquid transition. When FM particles are embedded in an elastomer, the elasticity of the composite is modulated by the phase of the embedded particles. On its own, FM is highly conductive, with a resistivity of 5.2×10^{-7} Ωm (about 31× that of copper). However, achieving the percolation threshold for electrical conductivity in a filler composite using only spherical particles is challenging without introducing other composite defects. The incorporation of high aspect ratio (HAR) particles reduces the percolation threshold for creating electrical pathways and, at the same time, increases the elastic modulus of the composite. In the following sections, we present fabrication methods for creating both spherical and HAR particles (fibers) of FM ranging from AR = 5.6 to 19.5 (**Figure 1**a,b), characterize the mechanical and electrical properties of silicone composites containing these particles, and demonstrate the application of a highly stretchable, variable stiffness, and electrically conductive composite in a robotic structure with reprogrammable actuation trajectories.

2. Results and Discussion

Increasing the AR of fibers in a composite material increases the material stiffness in composites with fixed filler contents[34,35] Figure 1c shows that if the volume content of the FM fillers is kept constant at 40%, the modulus of the composite containing the particles with AR = 19.5 is ≈2× the modulus of the composite containing the spherical FM inclusions. Because the incorporation of HAR particles in a composite matrix creates line contacts between the inclusions, in contrast to point contacts in the case of spherical inclusions, it also reduces the percolation threshold for creating conductive pathways[36] (Figure 1a), thereby enhancing electrical conductivity.[37–39] Figure 1c shows that at 40 vol% of FM inclusions, composites containing spherical particles (AR = 1) are not electrically

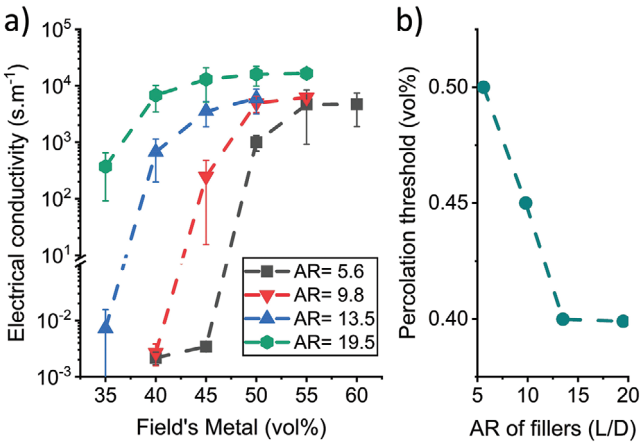

Figure 2. Electrical properties. a) Electrical conductivity of silicone composites containing FM inclusions with varying AR versus the volume content of the inclusions. Each data point is acquired based on testing five samples and error bars represent ±1 standard deviation. b) Percolation threshold of the silicone composites versus AR of inclusions obtained by fitting the data shown in (a) to the equation $\sigma = \sigma_0(V_f - V_c)^t$.[38]

conductive, while increasing the AR of fillers from 5.6 to 19.5 enhances the electrical conductivity of composites by ≈7 orders of magnitude.

When heated, FM inclusions undergo a solid–liquid phase change and the stiffness of the composite decreases. Figure 1d shows that strips of the variable stiffness composite containing either the spherical particles or HAR particles can hold a 100 g weight in their rigid state. The composite containing the spherical particles will need an external source of heat to soften, but the composite containing the HAR particles can be softened through Joule-heating on demand by applying an electrical current to both ends of the strip. Video S1 (Supporting Information) shows this softening process when the input power applied to both ends of the strip is 8 W (2 V and 4 A).

We systematically characterized the electrical conductivity and percolation thresholds of composites containing HAR particles. **Figure 2**a shows that by either increasing the vol% or the AR of fillers, the electrical conductivity of the composite increases. It can also be seen that the percolation threshold decreases with increasing the AR of fillers. The electrical conductivity of polymer composites obeys a power law dependence, $\sigma = \sigma_0(V_f - V_c)^t$, predicted by percolation theory for filler concentrations which is sufficiently close to the percolation threshold. Equation $\sigma = \sigma_0(V_f - V_c)^t$ only applies to the volume fractions greater than the percolation threshold, $V_f > V_c$, where V_f, V_c, σ_0, and t are the volume fraction of filler, the percolation threshold, a constant, and the critical exponent, respectively (See Supporting Information for more details).[38] The percolation threshold is ≈50 vol% when AR = 5.6, and it decreases to ≈40 vol% when the AR = 19.5 (Figure 2b).

Figure 3 compares the mechanical properties and electrical conductivity of the composites containing HAR particles with AR = 5.6 and 19.5 in rigid and soft states versus different volume fractions of FM inclusions. By increasing either the volume fraction or AR of FM fillers, both the elastic modulus and cold–hot modulus ratio are also increased (Figure 3a,b). Our results for elastic moduli of composites as cast in Figure 3a are in agreement with the theoretical results from the Halpin-Tsai and Guth (see Supporting Information for more details) composite models.[34,35] We find that Halpin-Tsai can reasonably model the elastic modulus of composites containing inclusions with AR = 19.5, which is in agreement with prior literature.[32] However, the model overestimates the modulus in composites containing inclusions with AR = 5.6, so the Guth model has been implemented to model the latter case.

If the composite is first softened and then strained to 150%, the oxide layer on the inclusions' surface will rupture, allowing the inclusions to reflow and coalesce to create an interconnected FM network. Subsequently, when the network structure cools and solidifies, the elastic modulus of the composite in the rigid state is increased even further. We chose 150% as the activation strain because all composites with different volume fractions of HAR FM particles were activated in our experiments beyond this threshold. The increase in the elastic modulus is not observed when the composites are softened but not strained, which we attribute to the presence of the thin oxide layer (≈4 nm, E =116 GPa[40]) at the surface of the particles. FM oxide is composed of ≈90 wt% indium oxide (In_2O_3), ≈10 wt% tin oxide (SnO_2), and a negligible amount of bismuth oxide (Bi_2O_3) in which indium oxide is the dominant chemical compound with a melting temperature at ≈1910 °C.[41] The failure strain of the oxide layer is dependent on its thickness and has been reported 0.003 for a 16.8 nm thick film.[42] Therefore, we surmise that the FM oxide does not melt, but rather a large strain must be applied in the soft state to break the oxide layer encompassing the molten core of the particles and "activate" the composites. This activation process also enhances the electrical conductivity in the composites and is more drastic, up to ≈5 orders of magnitude, for composites with lower content of the HAR FM inclusions (Figure 3c,d and Figure S1, Supporting Information).

We note that the experimental results for the elastic modulus of the composites containing particles with AR = 19.5 do not follow the trend predicted by Halpin-Tsai theoretical equations when the content of FM inclusions exceeds 55 vol% (shaded region in Figure 3a). We attribute this drop in the elastic modulus of the composites to an increasing presence of voids (Figure 3e), since the maximum packing fraction in a randomly dispersed 3D mixture decreases with increasing AR of inclusions.[37] The porosity of the composites has been calculated by weighing the samples with known dimensions and then comparing the density of the samples with the theoretical density obtained from the rule of mixtures. Figure 3e shows that the porosity of the composites including more than 55 vol% of FM particles with AR = 19.5 is more than 25%, which significantly affects the elongation at break of the composite at rigid and soft states. The elongation at break for composites containing inclusions with AR = 19.5, shown in Figure 3f, reduces by about 100% in the soft state when the FM content increases from 55 to 60 vol% and above.

Porosity further affects the stability of samples undergoing thermal cycling. The standard deviation of the elastic modulus of the activated composites reported in Figure 3a is less than 20% for all composites containing AR = 5.6 particles, and also for composites containing AR = 19.5 particles at FM volume fractions lower then 50%. This standard deviation, which is a measure of the soft-to-rigid reversibility of the composites, is directly affected by the porosity of the structure, as structures

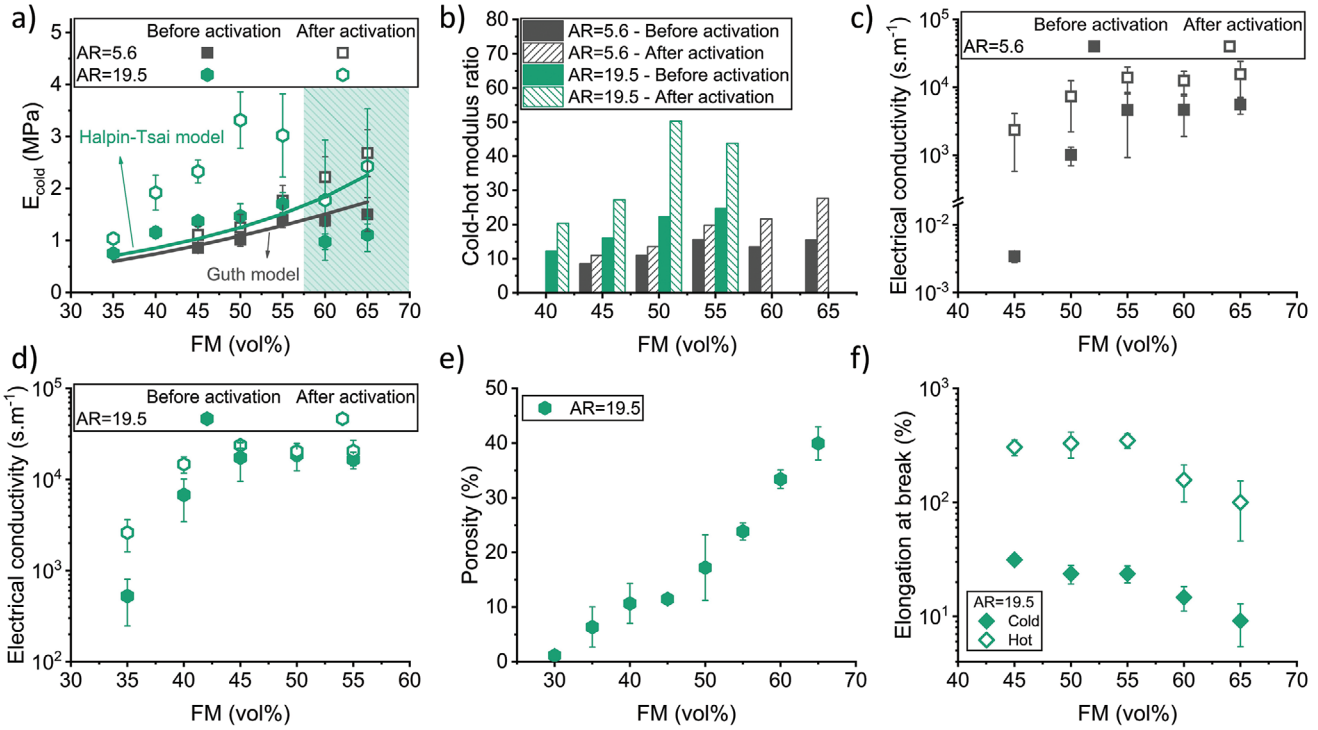

Figure 3. Comparing mechanical and electrical properties of composites containing FM inclusions with AR = 5.6 and 19.5. a) Elastic modulus of composites in the rigid state versus FM volume content before and after activation. The Halpin-Tsai (green line) and Guth (black line) theoretical models are in good agreement with the experimental results. Data points represent five samples that were each cycled five times between cold and hot states. b) Cold–hot modulus ratio of composites versus volume content of FM inclusions before and after activation. c) Electrical conductivity of composites versus volume content of FM inclusions with AR = 5.6 before and after activation. d) Electrical conductivity of composites versus volume content of FM inclusions with AR = 19.5 before and after activation. e) Porosity of the composite containing inclusions with AR = 19.5 versus the volume content of FM. f) Elongation at break versus volume fraction of FM inclusions with AR = 19.5 in the rigid and soft states. Error bars represent ±1 standard deviation.

with higher porosity are more prone to FM leakage and reduced soft-to-rigid reversibility. Figure S2 (Supporting Information) shows the elastic modulus of representative composite samples containing particles with AR = 19.5 after activation in the rigid and soft states.

Finally, we employ the results of our study to introduce a material that is both electrically conductive and possesses variable stiffness properties, which we apply to a soft inflatable cylindrical actuator to program its actuation trajectories via selective softening of the surface materials (**Figure 4**). The sidewall of the actuator was fabricated from a thin silicone membrane embedded with inextensible parallel threads, and both ends of the actuator were capped and sealed with laser-cut acrylic disks. The actuator could only extend in the longitudinal direction when pressurized due to constraints applied by the inextensible threads in the radial direction. Three composite strips, containing 50 vol% of FM inclusions with AR = 19.5, were located axisymmetrically around the sidewall of the actuator and glued using uncured silicone as the bonding agent (Figure 4a). The actuator was pressurized with 10 kPa air pressure and held its straight configuration when all the strips were in the rigid state (Figure 4b). When one of the strips was softened by applying 2.5 A electrical current, an average power rate of ≈0.005 W mm^{-3}, the sidewall under the compliant strip could extend, and as a result, the actuator bent toward the opposite direction (Video S2, Supporting Information). Figure 4c–e shows the actuator bending, with a curvature of ≈0.1 cm^{-1}, toward left, right, and back when the right, left, and front strips were softened, respectively.

3. Conclusions

We studied the effect of filler aspect ratio in phase-changing filler composites on modulus range and electrical conductivity. Based on these findings, the composite developed herein contains a single type of inclusion that contributes to both variable stiffness properties and electrical conductivity, allowing high mechanical strains (≈300% for V_f < 55%) when heated and softened. Incorporation of FM HAR particles substantially increases the cold-hot modulus ratio of the composite compared to the case of using spherical inclusions. Using HAR particles also reduces the percolation threshold for electrical conductivity, which is very challenging to achieve using spherical particles alone. Adjacent inclusions are in sufficient contact to create electrical pathways, and when the composite is softened and stretched for the first time, the inclusions coalesce and create longer structures, which further increases the elastic modulus of the composite in the cold state. For example, the cold–hot modulus ratio of a composite containing 55 vol% of FM inclusions with AR = 19.5 increased from ≈25 to ≈45 after activation. We showcased the application of this composite in controlling the trajectory of a soft body while

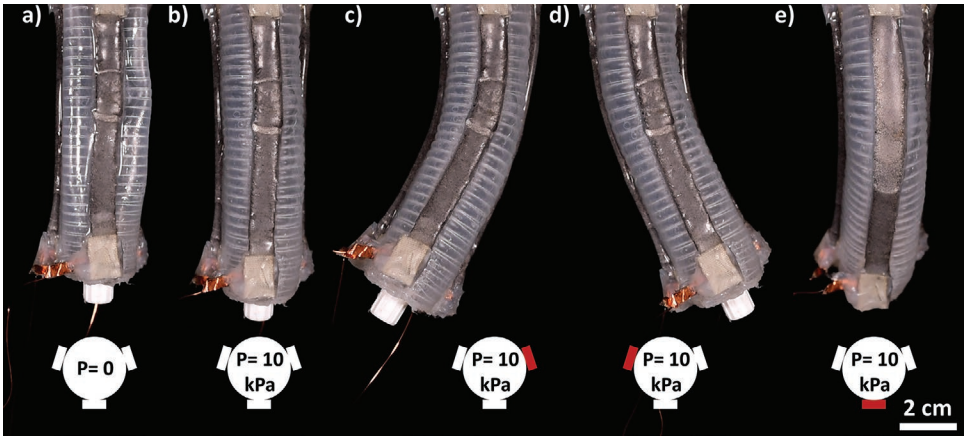

Figure 4. Three strips of the composite are positioned and glued axisymmetrically around the sidewall of an inflatable cylindrical actuator (a). The actuator is made of a silicone membrane with embedded inextensible parallel threads to constrain the radial expansion of the structure. When all the composite strips are in the rigid state and the actuator is pressurized with 10 kPa air pressure (b), the actuator holds its straight configuration. However, when the right, left or front strip is softened, the actuator bends toward c) left, d) right, or e) back, respectively. The red strip in the schematic shows the location of the compliant strip.

being softened with electrical current on-demand. We expect that HAR phase-changing fillers will be widely used in the future for creating stiffness tunable composites in robotics due to their ease of implementation and manufacture.

4. Experimental Section

Fabrication and Characterization of HAR Particles: The fabrication process of the HAR FM particles is illustrated in Figure S3, Supporting Information. An ingot of FM (Roto144F, RotoMetals, Inc.) was submerged in a 200 mL glass beaker filled with deionized water and the mixture was heated up on a hot plate for ≈20 min at 100 °C to melt the FM. In the next step, a 3 mL syringe was used to collect 2 mL of the molten metal and the hot water. A blunt tip needle with the appropriate inner diameter (50 to 270 μm) was inserted on the syringe tip, and the contents of the syringe were injected into a 500 mL beaker containing water at room temperature. In this process, long fibers of FM were created due to the instant solidification of the molten metal stream entering the cold water. The above procedure was repeated till all the molten FM content was collected with the syringe and transformed into long FM fibers. Next, a mechanical homogenizer (Cole-Pramer LabGEN 850) with a 20 mm diameter saw-tooth generator attachment was inserted into the mixture of the water and long FM fibers at 5000 rpm for 30 s to smash the long FM fibers into short FM fibers (HAR particles). The supernatant was removed from the beaker and the particles were dried in a vacuum oven at 55 °C for ≈12 h to remove as much of the remaining moisture as possible. The resulting dry particles may agglomerate together like sandstone and needed to be shaken apart and sieved. AR of the particles was controlled by the inner diameter of the needle used for injecting the molten FM into cold water. The clearance between the stator and rotor of the homogenizer saw-tooth generator was fixed at ≈0.7 mm and therefore was not actively used to modulate the AR of the particles. The length and diameter of the particles were measured using the visual processing software ImageJ, and AR was calculated as length/diameter for each individual particle. Length was measured along the full curve of a given particle as the particles were not always straight. The average ARs and the standard deviations for different batches are reported in Figure 1b.

Fabrication of Spherical Particles: Spherical particles were manufactured via a process modified from ref. [43]. An ingot of FM (Roto144F, RotoMetals, Inc.) was submerged in a 500 mL glass beaker filled with 200 mL of a thixotropic mixture, made from an aqueous solution of confectionery sodium alginate powder with a loading of 2 wt%. The mixture was then warmed up to ≈70 °C by placing the beaker inside of a heated oil bath (95 °C). Once fully melted, the FM ingot was broken apart using a mechanical homogenizer (Cole-Parmer LabGEN 850) with a 20 mm diameter saw-tooth generator attachment for 60 s at a specified rpm depending on the particle size desired (higher rpms corresponded with smaller diameter particles). After homogenization, the medium shear-thickened in place, which prevented the Field's metal droplets from settling or aggregating while they were allowed to cool. The mixture was then diluted in a large container by stirring in additional water, at which point the FM particles were able to settle and collect at the bottom of the container. The supernatant was removed from the beaker and the particles were dried in a vacuum oven at 55 °C for ≈12 h to remove as much of the remaining moisture as possible. The resulting dry particles may agglomerate together like sandstone and needed to be shaken apart and sieved.

Fabrication of Composite: HAR FM particles and Ecoflex 30 (Smooth-on Inc.) were hand-mixed for ≈1 min to distribute the particles evenly throughout the silicone matrix. The mixture was then cast into acrylic molds with appropriate dimensions for the mechanical and electrical testing. The molds were placed in a vacuum oven at room temperature for 2 min to degas the mixture. Next, the samples were cured in an oven at 60 °C for 12 hs.

Fabrication of Inflatable Cylindrical Actuator: The cylindrical actuator was made by first creating a thin silicone (EcoFlex 30, Smooth-On) membrane with embedded parallel polyester threads at 3 mm spacing, and then wrapping the membrane into a cylinder of 1-inch diameter. The membrane was positioned in a way that the inextensible threads constrained the expansion of the actuator in the radial direction. Acrylic caps with holes were laser-cut and Luer lock connectors were glued to the caps using instant adhesive (Loctite 401). The acrylic caps were then attached on both ends of the cylinder with silicone adhesive (Sil-poxy, Smooth-On). The detailed fabrication process of the silicone membrane embedded with the inextensible treads is described in previous work.[44] Three 90mm × 10mm × 3 mm composite strips were then positioned axisymmetrically around the sidewall of the actuator and glued using Ecoflex 30 as the bonding agent. Copper shims were wrapped around both ends of the composite strips to be used as electrodes. One drop of liquid metal (eGaIn) was used between the electrodes and the composite to reduce the contact resistance between the strips and the copper electrodes. Fabric reinforcements were added over the electrode sites to create a strain-free region to provide reliable electrical connections.

Mechanical Testing: For stiffness characterization, tensile testing was conducted on 50mm × 10mm × 3 mm rectangular samples of

the FM-Ecoflex 30 composite using an Instron 3345 testing system equipped with a 50 N load cell. Fabric reinforcements were adhered to both ends of each sample for enhancing the grip in the Instron machine, which resulted in a stretchable portion of 30mm × 10mm × 3 mm for each sample. The samples were loaded in tension with a constant displacement rate of 2 mm min^{-1}, up to a strain of 5%, and then unloaded to the stress-free state. Bluehill Universal testing software was used to automatically calculate the elastic moduli of samples from the stress–strain measurements.

Electrical Testing: Strips of copper shim were wrapped around the ends of each 60mm × 5mm × 2 mm rectangular sample of the FM-Ecoflex 30 composite, resulting in a stretchable portion of 50mm × 5mm × 2 mm. The samples were left in an oven at 80 °C for 15 min and then both ends were slightly squeezed to enhance the electrical connection between the copper stripes and the FM inclusions. The samples were placed inside a Petri dish and uncured Ecoflex 30 were poured into the Petri dish to submerge the samples, such that they can be embedded in a thin skin of silicone on both sides to prevent melted FM leaking in later steps. Next, the Petri dish was left in an oven at 60 °C for 6 h. Finally, the samples were carved out of the cured sheet. A four-point probe technique was adopted to measure the electrical resistivity of the samples using a digital multimeter (BK Precision 5492B) at room temperature in two different scenarios of 1) the pristine state and 2) after stretching the samples up to 150% for the first time in the soft state and releasing them to come back to their original lengths and cooling down.

Supporting Information

Supporting Information is available from the Wiley Online Library or from the author.

Acknowledgements

This material is based upon work supported by the National Science Foundation under Grant No. EFMA-1830870.

Conflict of Interest

The authors declare no conflict of interest.

Data Availability Statement

The data that support the findings of this study are available from the corresponding author upon reasonable request.

Keywords

conductive composite, shape morphing, variable elasticity, variable stiffness

Received: July 23, 2021
Revised: August 30, 2021
Published online:

[1] L. Wang, Y. Yang, Y. Chen, C. Majidi, F. Iida, E. Askounis, Q. Pei, *Mater. Today* **2018**, *21*, 563.
[2] N. G. Cheng, A. Gopinath, L. Wang, K. Iagnemma, A. E. Hosoi, *Macromol. Mater. Eng.* **2014**, *299*, 1279.
[3] M. Tatari, A. Mohammadi Nasab, K. T. Turner, W. Shan, *Adv. Mater. Interfaces* **2018**, *5*, 1800321.
[4] S. Sharifi, C. Rux, N. Sparling, G. Wan, A. Mohammadi Nasab, A. Siddaiah, P. Menezes, T. Zhang, W. Shan, *Front. Robot. AI* **2021**, *8*, 191.
[5] L. Blanc, A. Delchambre, P. Lambert, *Actuators* **2017**, *6*, 23.
[6] C. Majidi, R. J. Wood, *Appl. Phys. Lett.* **2010**, *97*, 164104.
[7] G. Aydar, X. Wang, F. Gordaninejad, *Smart Mater. Struct.* **2010**, *19*, 6.
[8] Y. Li, Y. Maeda, M. Hashimoto, *Int. J. Adv. Robot. Syst.* **2015**, *12*, 1751.
[9] A. M. Nasab, A. Sabzehzar, M. Tatari, C. Majidi, W. Shan, *Soft Rob.* **2017**, *4*, 411.
[10] D. Shah, B. Yang, S. Kriegman, M. Levin, J. Bongard, R. Kramer-Bottiglio, *Adv. Mater.* **2020**, *33*, 2002882.
[11] D. S. Shah, E. J. Yang, M. C. Yuen, E. C. Huang, R. Kramer-Bottiglio, *Adv. Funct. Mater.* **2021**, *31*, 2006915.
[12] T. L. Buckner, R. A. Bilodeau, S. Y. Kim, R. Kramer-Bottiglio, *Proc. Natl. Acad. Sci. USA* **2020**, *117*, 25360.
[13] E. Brown, N. Rodenberg, J. Amend, A. Mozeika, E. Steltz, M. R. Zakin, H. Lipson, H. M. Jaeger, *Proc. Natl. Acad. Sci. U. S. A.* **2010**, *107*, 18809.
[14] Y. Shan, M. Philen, A. Lotfi, S. Li, C. E. Bakis, C. D. Rahn, K. W. Wang, *J. Intell. Mater. Syst. Struct.* **2009**, *20*, 443.
[15] U. C. Jeong, J. H. Yoon, I. H. Yang, J. E. Jeong, J. S. Kim, K. H. Chung, J. E. Oh, *Smart Mater. Struct.* **2013**, *22*, 11.
[16] J. S. Oh, Y. M. Han, S. R. Lee, S. B. Choi, *Smart Mater. Struct.* **2013**, *22*, 4.
[17] C. Cao, X. Zhao, *Appl. Phys. Lett.* **2013**, *103*, 4.
[18] A. Firouzeh, M. Salerno, J. Paik, *IEEE Trans. Robot.* **2017**, *33*, 765.
[19] X. Huang, K. Kumar, M. K. Jawed, A. M. Nasab, Z. Ye, W. Shan, C. Majidi, *Sci. Robot.* **2018**, *3*, 7557.
[20] X. Huang, K. Kumar, M. K. Jawed, A. Mohammadi Nasab, Z. Ye, W. Shan, C. Majidi, *Adv. Mater. Technol.* **2019**, *4*, 1800540.
[21] G. McKnight, R. Doty, A. Keefe, G. Herrera, C. Henry, *J. Intell. Mater. Syst. Struct.* **2010**, *21*, 1783.
[22] M. J. Ford, C. P. Ambulo, T. A. Kent, E. J. Markvicka, C. Pan, J. Malen, T. H. Ware, C. Majidi, *Proc. Natl. Acad. Sci. USA* **2019**, *116*, 21438.
[23] P. Lv, X. Yang, H. K. Bisoyi, H. Zeng, X. Zhang, Y. Chen, P. Xue, S. Shi, A. Priimagi, L. Wang, W. Feng, Q. Li, *Mater. Horiz.* **2021**, *8*, 2475.
[24] Y. Chen, J. Yang, X. Zhang, Y. Feng, H. Zeng, L. Wang, W. Feng, *Mater. Horiz.* **2021**, *8*, 728.
[25] T. L. Buckner, M. C. Yuen, S. Y. Kim, R. Kramer-Bottiglio, *Adv. Funct. Mater.* **2019**, *29*, 1903368.
[26] T. L. Buckner, M. C. Yuen, R. Kramer-Bottiglio, in *3rd IEEE Int. Conf. on Soft Robotics (RoboSoft)*, IEEE, Piscataway, NJ **2020**, pp. 259–265.
[27] S. I. Rich, R. J. Wood, C. Majidi, *Nat. Electron.* **2018**, *1*, 102.
[28] A. Tonazzini, S. Mintchev, B. Schubert, B. Mazzolai, J. Shintake, D. Floreano, *Adv. Mater.* **2016**, *28*, 10142.
[29] W. Shan, T. Lu, C. Majidi, *Smart Mater. Struct.* **2013**, *22*, 085005.
[30] W. Shan, S. Diller, A. Tutcuoglu, C. Majidi, *Smart Mater. Struct.* **2015**, *24*, 065001.
[31] T. L. Buckner, E. L. White, M. C. Yuen, R. A. Bilodeau, R. K. Kramer, in *IEEE Int. Conf. on Intelligent Robots and Systems*, IEEE, Piscataway, NJ **2017**, pp. 3728–3733.
[32] A. Mohammadi Nasab, S. Sharifi, S. Chen, Y. Jiao, W. Shan, *Adv. Intell. Syst.* **2020**, *3*, 2000166.
[33] I. M. Van Meerbeek, B. C. Mac Murray, J. W. Kim, S. S. Robinson, P. X. Zou, M. N. Silberstein, R. F. Shepherd, *Adv. Mater.* **2016**, *28*, 2801.
[34] R. Gibson, *Principles of Composite Material Mechanics, 4th ed.*, CRC Press, Boca Raton, FL **2016**.
[35] E. Guth, *J. Appl. Phys.* **1945**, *16*, 20.
[36] R. A. Bilodeau, A. Mohammadi Nasab, D. S. Shah, R. Kramer-Bottiglio, *Soft Matter* **2020**, *16*, 5827.
[37] D. M. Bigg, *Adv. Polym. Technol.* **1984**, *4*, 255.

[38] M. Loos, in *Carbon Nanotube Reinforced Composites: CNR Polymer Science and Technology*, Elsevier, New York **2015**, pp. 125–170.
[39] W. Bauhofer, J. Z. Kovacs, *Compos. Sci. Technol.* **2009**, *69*, 1486.
[40] D. Neerinck, T. Vink, *Thin Solid Films* **1996**, *278*, 12.
[41] S. A. Idrus-Saidi, J. Tang, M. B. Ghasemian, J. Yang, J. Han, N. Syed, T. Daeneke, R. Abbasi, P. Koshy, A. P. O'Mullane, K. Kalantar-Zadeh, *J. Mater. Chem. A* **2019**, *7*, 17876.
[42] D. R. Cairns, D. C. Paine, G. P. Crawford, *M RS Proc.* **2001**, *666*, F3.24.
[43] S. Y. Kim, S. Liu, S. Sohn, J. Jacobs, M. D. Shattuck, C. S. O'Hern, J. Schroers, M. Loewenberg, R. Kramer-Bottiglio, *Nat. Commun.* **2021**, *12*, 3768.
[44] S. Y. Kim, R. Baines, J. Booth, N. Vasios, K. Bertoldi, R. Kramer-Bottiglio, *Nat. Commun.* **2019**, *10*, 3464.